Design and synthesis of 4-amino-2',4'-dihydroxyindanone derivatives as potent inhibitors of tyrosinase and melanin biosynthesis in human melanoma cells

Leticia M. Lazinski,[1,2] Morane Beaumet,[1] Brayan Roulier,[1] Rémy Gay,[1] Guy Royal,[2] Marc Maresca[3] and Romain Haudecoeur*[,1]

1. Univ. Grenoble Alpes, CNRS, DPM, 38000 Grenoble, France.
2. Univ. Grenoble Alpes, CNRS, DCM, 38000 Grenoble, France.
3. Aix Marseille Univ., CNRS, Centrale Marseille, iSm2, 13013 Marseille, France.

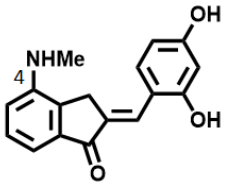

IC_{50} = 14 nM (*ab*TYR)
IC_{50} = 890 nM
(MNT-1 lysates)
IC_{50} = 770 nM
(MNT-1 cells, 14 d)

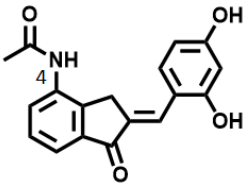

IC_{50} = 8.6 nM (*ab*TYR)
IC_{50} = 140 nM
(MNT-1 lysates)
IC_{50} = 3,300 nM
(MNT-1 cells, 14 d)

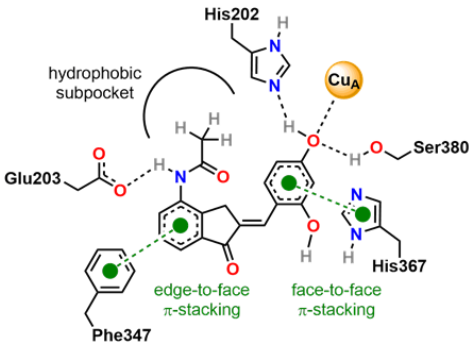

ABSTRACT

Melanogenesis inhibition constitutes a privileged therapeutic solution to treat skin hyperpigmentation, a major dermatological concern associated with the overproduction of melanin by human tyrosinase (*hs*TYR). Despite the existence of many well-known TYR (tyrosinase) inhibitors commercialized in skin formulations, their *hs*TYR-inhibition efficacy remains poor since most of them were investigated over mushroom tyrosinase (*ab*TYR), a model with low homology relative to *hs*TYR. Considering the need for new potent *hs*TYR inhibitors, we

designed and synthesized a series of indanones starting from 4-hydroxy compound **1a**, one of the two most active derivatives reported to date against the human enzyme, together with marketed thiamidol. We observed that analogues featuring 4-amino and 4-amido-2',4'-dihydroxyindanone motifs showed two- to ten-fold increase in activity over human melanoma MNT-1 cell lysates, and a ten-fold improvement in a 4-days whole-cell experiment, compared to parent analogue **1a**. Molecular docking investigation was performed for the most promising 4-amido derivatives and suggested a plausible interaction pattern with the second coordination sphere of *hs*TYR, notably through hydrogen bonding with Glu203, confirming their impact in the binding mode with *hs*TYR active site.

Keywords: tyrosinase, indanone, melanogenesis, melanoma, thiamidol, resorcinol

INTRODUCTION

Human tyrosinase (*hs*TYR, EC 1.14.18.1) is the key enzyme of human melanogenesis, a cutaneous process producing the main skin pigment melanin, as it catalyzes the rate-limiting first two steps of the biochemical pathway, *i.e.*, the *ortho*-hydroxylation of L-tyrosine followed by the oxidation of the resulting L-DOPA into dopaquinone.[1] More generally, *hs*TYR is able to assume the oxidation of a wide range of monophenolic and diphenolic substrates, due to its coupled dicopper active site.[2] Historically, *hs*TYR has long been seen as an ideal target for developing chemical agents intended to modulate or suppress melanin formation *in vivo*,[3] but the enzyme is costly and difficult to produce at high scale due to its complex and mammal-specific post-translational maturation process. Thus, a very large number of molecules were identified as tyrosinase inhibitors mostly on the sole basis of simple assays involving the cheap and readily available mushroom tyrosinase from *Agaricus bisporus* (*ab*TYR), with the implicit

assumption that the results would easily transpose in a human context.[4] The advances made within the past ten years in the structural knowledge and expression of *hs*TYR have demonstrated the opposite: most of the well-known TYR inhibitors described in the literature and widely used as positive references (*e.g.*, kojic acid, hydroquinone, arbutin) showed a 100- to 1000-times lower efficiency against the human enzyme, due to considerable differences in the respective interaction patterns at the active site.[5,6] Thus, true *hs*TYR inhibitors are missing and the dermocosmetic agents available for depigmentation purposes are used at high concentrations, providing global low activities and triggering severe side effects.[7] In addition, as melanin is known to play a crucial role in the high resistance of melanoma to classical anticancer therapies, powerful *hs*TYR inhibitors could be used as adjuvants for restoring the sensitivity of melanoma cells to radio- and/or chemotherapy, with the aim to improve the currently poor treatment outcome.[8–10] The recent years have witnessed advances in the expression, purification and structural knowledge of *hs*TYR, thereby opening new avenues for filling this void.[4,11,12] Thus, a pioneer generation of genuine *hs*TYR inhibitors emerged. Among them, the two most active molecules shared a K_i value of 0.25 µM using the isolated human enzyme, *i.e.*, thiamidol and compound **1a** (Figure 1). Thiamidol was developed by Beiersdorf and its *in vitro* potential was further confirmed by studies performed in a clinical context, yielding promising results in the frame of facial melasma treatment and leading to its commercial use as a skin-whitening agent in dermocosmetic preparations.[6,13,14] Indanone **1a** was identified through an iterative pharmacomodulation process started ten years ago, initially focused on the aurone backbone.[15–19] However, despite its superior affinity for isolated *hs*TYR, it was far less active in a cellular context, providing room for further improvement of its *in cellulo* and *in vivo* effects.

Compound **1a** featured a phenol group at position 4, which was hypothesized to form a crucial hydrogen bond with Glu203 from *hs*TYR second sphere of coordination.[19] On this basis, we designed and synthesized eighteen new compounds (**1b**–**s**) relying on the indanone scaffold,

which has already shown many biological activities,[20] with various substituents at position 4, especially by introducing several hydrogen-bond-donating amino or amido groups. The highly beneficial copper-binding resorcinol moiety was maintained at the B-ring, as it usually leads to genuine inhibitor behaviors, in contrast with phenol and catechol binding groups, as recently demonstrated by the thiamidol development.[6] The compounds were evaluated using both *ab*-TYR, *hs*TYR from human melanoma MNT-1 lysates, and whole human melanoma cells in order to validate the efficient transposition of their mushroom tyrosinase inhibitory effect in human cell-free and cell-based contexts, and to compare their potencies with that of the reference thiamidol. The binding geometry of indanones was then explored through molecular docking using a homology model of *hs*TYR.

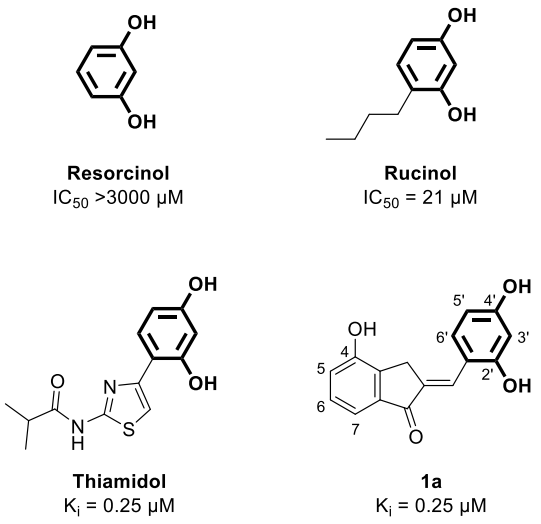

Figure 1. Structures of resorcinol-based *hs*TYR inhibitors, and numbering of the indanone scaffold.

RESULTS AND DISCUSSION

Chemical synthesis. The synthetic route for the studied compounds is depicted in Scheme 1. As a first common step, 4-aminoindanone derivatives were prepared from commercially available 4-nitroindanone **2h**, which was conveniently reduced to the amino counterpart **2i** in the

presence of Fe/NH_4Cl.[21] Then, compound **2i** underwent reactions with various anhydrides to afford amides **2l**–**p** with moderate to good yields. Boc-protection of intermediate **2i** was followed by reaction with MeI and NaH to produce the monomethylated derivative Boc-**2j**, while the dimethylated version **2k** was successfully obtained through reductive amination. The synthesis of intermediates Boc-**2q**–**s** was accomplished by reacting **2i** with the corresponding Boc-protected amino acid using DCC as coupling agent in the presence of HOBt. Lastly, 4-methyl-2,3-dihydro-1*H*-inden-1-one (**2c**) was obtained through intramolecular Friedel-Crafts acylation using trifluoromethanesulfonic acid as catalyst. All the other intermediates **2** were derived from commercial indanones. In most cases, the synthesis of the final 2,4-dihydroxyindanone backbone was performed by aldol condensation with 2,4-dimethoxybenzaldehyde in an alkaline medium and by a subsequent methoxy deprotection using BBr_3, following an already reported procedure.[22] Alternatively, the synthesis of analogues **1b**, **1h** and **1k** was found to be incompatible with BBr_3-mediated methoxy deprotection conditions and thus corresponding **2b**, **2h** and **2k** were directly condensed with 2,4-dihydroxybenzaldehyde in an acidic medium.

Scheme 1. Synthesis of indanones 1b–s.[a]

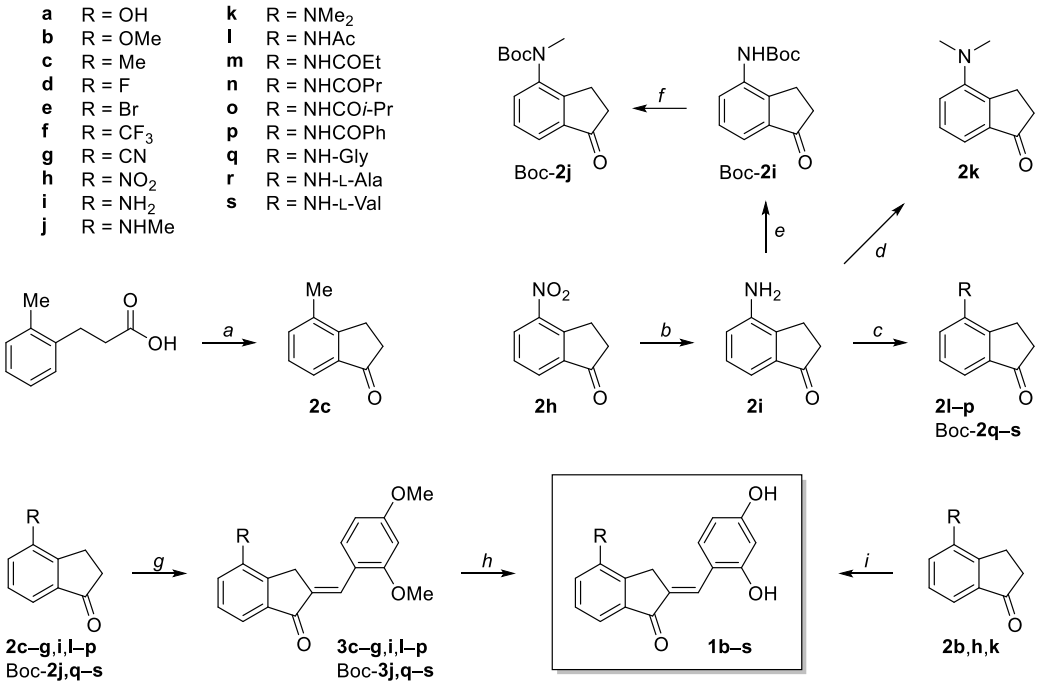

[a]Reagents and conditions: (a) trifluoromethanesulfonic acid, 25 °C; (b) Fe, NH_4Cl, EtOH, H_2O, 80 °C; (c) anhydride derivative, EtOAc, reflux, *or* Boc-protected amino acid, HOBt, DCC, CH_2Cl_2, 25 °C; (d) HCHO, $NaBH_4$, H_2SO_4, THF, H_2O, 25 °C; (e) Boc_2O, MeOH, reflux; (f) MeI, NaH, DMF, 25 °C; (g) 2,4-dimethoxybenzaldehyde, NaH, MeOH, 25 °C; (h) BBr_3, CH_2Cl_2, 25 °C; (i) 2,4-dihydroxybenzaldehyde, $SOCl_2$, MeOH.

Inhibition of *ab*TYR and *hs*TYR from MNT-1 cell lysates. As stated previously, directly applying results from *ab*TYR to human-directed applications often appears as a dubious extrapolation. Thus, all the synthesized compounds were tested against both purified *ab*TYR, in order to assess their ability to interact with an isolated tyrosinase, and *hs*TYR from human melanoma MNT-1 cell lysates, in order to confirm their effect in a human system. A classical colorimetric test was employed to detect the oxidation of the natural substrate L-DOPA. In the *ab*TYR assay, a readout at 475 nm was used for tracking dopachrome production, while the *hs*TYR-containing lysates assay measured the production of melanogenesis intermediates at

600 nm, in order to avoid interferences with the absorption properties of indanones as much as possible. Overall, the results tend to confirm the previously reported observations that *ab*TYR is a less restrictive enzyme than *hs*TYR, with a higher tolerance to steric hindrance and substituent switch. Indeed, while reference kojic acid (KA, Table 1) provided an IC_{50} of 33 µM against *ab*TYR, all the evaluated indanones fell in the submicromolar range, with some variations however. Compounds **1c**, **1j**, **1l**, **1m** and **1n** were especially found as nanomolar inhibitors of *ab*TYR, **1n** showing the lowest IC_{50} value among the series (IC_{50} = 6.3 nM). In contrast, activities recorded in the *hs*TYR inhibition assay performed using MNT-1 cell lysates yielded IC_{50} values spanning from less than 0.14 µM to greater than 100 µM, depending on the nature and bulkiness of the substituent at position 4. Interestingly, similar trends appear regarding the most active compounds, as amides **1l**–**n** yielded the lowest IC_{50} values in both assays. Indeed, while the introduction of various simple substituents at position 4, such as a methyl, fluoro, bromo, trifluoromethyl, cyano or nitro groups (compounds **1c**–**h**), led to moderately active or inactive derivatives with IC_{50} >9 µM against *hs*TYR from MNT-1 lysates (methoxy compound **1b** being a notable exception), the introduction of amine or amide groups significantly increased the inhibition potency. 4-Amino analogues **1i** and **1j** reached similar values under the micromolar range (IC_{50} = 0.72 µM and 0.89 µM, respectively), showing a twofold improvement compared to 4-hydroxy parent compound **1a**.[19] However, disubstituting the amino group triggered a striking drop of inhibition activity (IC_{50} = 24 µM), that possibly originated from the loss of any potential hydrogen-bond interactions at this position. The further modification of the 4-amino group into corresponding amides was overall beneficial. The linear aliphatic amides demonstrated superior outcomes, exhibiting IC_{50} values between 0.14 µM and 0.18 µM for the acetyl, propionyl, and butyryl variations, while branched and aromatic derivatives displayed lower inhibitory potency (IC_{50} = 0.35 µM for isobutyryl **1o** and 4.4 µM for phenyl **1p**). The inclusion of small amino acids also yielded generally unsatisfactory results, affording IC_{50} values ranging

from 0.85 µM to 3.2 µM for analogues **1q**, **1r** and **1s** based on glycine, L-alanine, and L-valine respectively. Collectively, these observations suggested a constrained steric tolerance at this position for larger chemical groups, extending beyond simple aliphatic chains. Overall, the whole pharmacomodulation process enabled a tenfold increase in terms of inhibition activity (IC_{50} = 0.14 µM for **1l**), compared to parent compound **1a** (IC_{50} = 1.6 µM),[19] and a two-order-of-magnitude improvement since the initial hit embedding a 2-hydroxypyridine-*N*-oxide moiety (IC_{50} = 15 µM).[18] Hence, compounds **1l**–**n** exhibited comparable activity to the reference thiamidol (IC_{50} = 0.17 µM), which is recognized as one of the most potent inhibitors of *hs*TYR reported to date.

Table 1. Structures and activities of indanone derivatives 1a–s against *ab*TYR and *hs*TYR from human melanoma MNT-1 cell lysates.

compound	R	*ab*TYR IC_{50} (μM)	*hs*TYR in cell lysates IC_{50} (μM)
1a	OH	0.09 ± 0.02	1.6 ± 0.2[19]
1b	OMe	0.16 ± 0.02	1.8 ± 0.1
1c	Me	0.0190 ± 0.0009	15 ± 3
1d	F	0.15 ± 0.01	9 ± 1
1e	Br	0.086 ± 0.008	66 ± 5
1f	CF_3	0.18 ± 0.02	>100
1g	CN	0.26 ± 0.02	50 ± 20
1h	NO_2	0.16 ± 0.02	>100
1i	NH_2	0.027 ± 0.007	0.72 ± 0.08
1j	NHMe	0.014 ± 0.001	0.89 ± 0.05
1k	NMe_2	0.083 ± 0.008	24 ± 3
1l	NHAc	0.0086 ± 0.0008	0.14 ± 0.01
1m	NHCOEt	0.014 ± 0.002	0.15 ± 0.02
1n	NHCOPr	0.0063 ± 0.0007	0.18 ± 0.04
1o	NHCO*i*-Pr	0.06 ± 0.01	0.35 ± 0.06
1p	NHCOPh	0.10 ± 0.03	4.4 ± 0.6
1q	NH-Gly	0.39 ± 0.08	2.0 ± 0.2
1r	NH-L-Ala	0.6 ± 0.2	0.85 ± 0.01
1s	NH-L-Val	0.46 ± 0.09	3.2 ± 0.3
Kojic acid	—	33 ± 4	>100
Thiamidol	—	—	0.17 ± 0.05

Molecular modeling of *hs*TYR–inhibitors interactions. Due to its transmembrane and highly glycosylated nature, *hs*TYR crystallization attempts failed to produce tridimensional structures at atomic level to date. However, since 2017 and the publication of the crystal structure of closely-related *hs*TYRP1,[23] which shares 44% of identity with *hs*TYR, a *hs*TYRP1-based homology model of *hs*TYR is accessible[24] and outperforms previous builds that relied on mushroom and/or plant polyphenol oxidases as templates. A recent report highlighted the superior accuracy achieved by the docking software LeDock when applied to metalloproteins,[25] and thus

we chose to use this software for exploring indanones' binding geometry inside *hs*TYRP1-based *hs*TYR model active site. In general, the best poses obtained for 4-amido compounds exhibited remarkable similarity, as illustrated by the superimposition of poses from **1l**, **1m** and **1n** (Figure 2F), and were reminiscent of the geometry observed in the case of parent molecule **1a**.[19] Multiple interactions seem to maintain the compounds into the active site, as seen in Figures 2A and 2C with the example of **1l**. The binding of the 4'-OH group to the copper atom A was expected, as it was also seen in previous studies. In this case, His202 may play a role by forming a hydrogen bond with 4'-OH, possibly assisting the deprotonation of this group prior to metal binding, as already described in the detailed mechanism of L-tyrosine approach during catalysis.[26] In addition, it appeared that the hydroxy group is stabilized in its position by the hydrogen bond donating effect of the nearby Ser380 residue, not conserved in *ab*TYR. As observed for natural substrates L-tyrosine and L-DOPA, the approach of inhibitors may be facilitated by the face-to-face π-stacking effect involving copper-coordinating His367. Similar effects were seen upon examination of reported crystal structures of substrate–Zn-soaked-TYR complexes,[27] and therefore superimposing L-tyrosine and L-DOPA from these structures (PDB id 4P6R and 4P6S, respectively) with the best docking pose obtained with **1l** resulted in a nearly perfect alignment of the copper-interacting phenyl rings and hydroxy groups, as depicted in Figures 2D and 2E, respectively. Nevertheless, the rest of the indanone structure seems to fully participate to the binding geometry by establishing interactions with remote residues. An additional edge-to-face π-stacking interaction occurred in all the best poses between the indanone A-ring and Phe347, while a hydrogen bond between the 4-NH group and Glu203 appeared to orient the inhibitors into the binding site, akin to what was observed in the case of parent **1a**.[19] The latter point could account for the significant variations in measured activity between **1i**–**j** (IC_{50} = 0.72–0.89 µM) and **1k** (IC_{50} = 24 µM). Finally, the insertion of a small linear aliphatic chain (*i.e.*, methyl **1l**, ethyl **1m** and propyl **1n**) through a 4-amido group could contribute to fill

a previously unexplored hydrophobic subpocket, mainly formed by Asp199, Val377 and several amino acid main chains (Figure 2B).

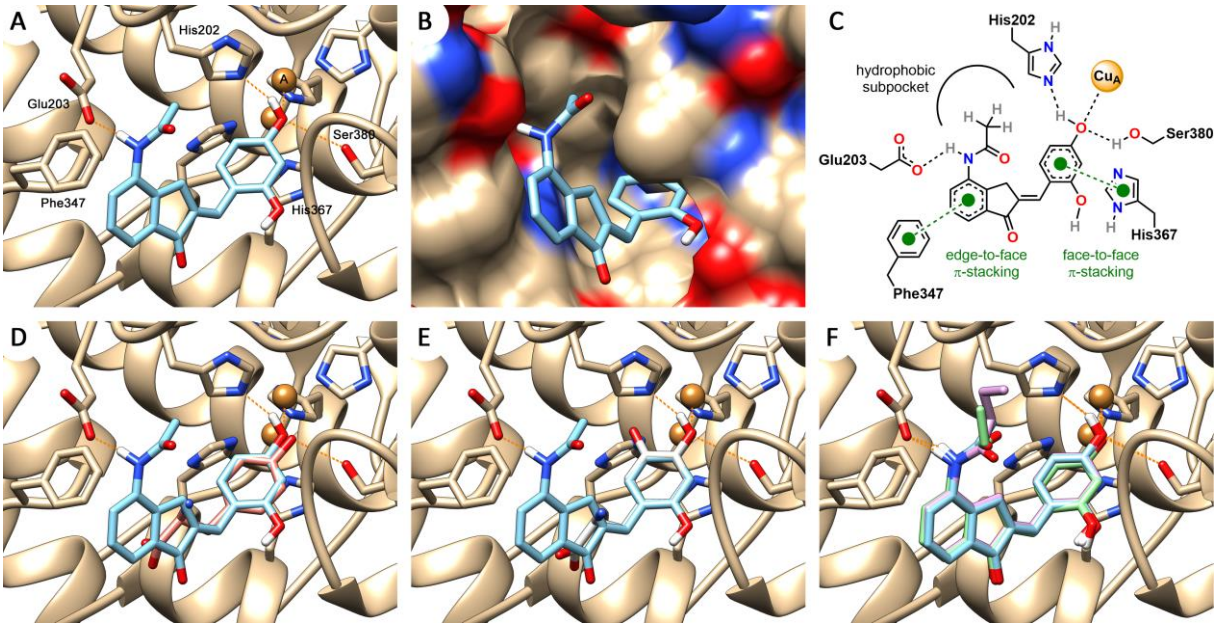

Figure 2. Representations of predicted binding modes of indanones at the active site of a *hs*TYR homology model, provided by LeDock software. (A–B) Best pose obtained with compound **1l** (blue) in a cartoon or surface protein representation. (C) Schematic view of key interactions predicted for the **1l**-*hs*TYR complex. (D–E) Superimpositions of L-tyrosine (pink) and L-DOPA (white) from previously reported *hs*TYR crystal structures with the best pose of compound **1l** docked at the active site of *hs*TYR. (F) Superimposition of the best poses obtained with **1l**, **1m** (green) and **1n** (purple) at the active site of *hs*TYR.

Suppression of melanogenesis in MNT-1 human melanoma cells. Beyond the ability of tested indanones to inhibit human and mushroom tyrosinases in cell-free environments, our next step was to assess their potential as melanogenesis suppressors in human melanoma cells. To achieve this, we carried out further experiments involving MNT-1 whole cells using the best-performing compounds identified in the *hs*TYR inhibition assay, namely, **1c**, **1i**, **1j**, **1l**–**o**, **1q** and **1r**. Kojic acid and thiamidol were included as negative and positive references,

respectively. MNT-1 cells were exposed to increasing concentrations of molecules for either 4 or 14 days, similarly to the conditions used to demonstrate thiamidol's melanogenesis inhibition potency in human melanocytes.[6] The cytotoxicity of evaluated compounds was assessed through resazurin assay whereas the inhibition of melanin synthesis was measured through quantification of intracellular melanin following cell lysis. After 4-days exposure, most of the derivatives exhibited minimal toxicity at concentrations below 100 µM, representing an improvement compared to previously described **1a** (CC_{50} = 91 µM, Table 2). Compound **1j** displayed slightly higher cytotoxicity (CC_{50} = 78 µM), but it remained within the range suitable for low micromolar operations. In terms of melanogenesis suppression efficiency, the majority of indanones were more active than parent compound **1a** (IC_{50} = 3.2–29 µM, *vs.* 29 µM, respectively), consistent with the results obtained with MNT-1 cell lysates. While compounds **1c**, **1l**, **1n**, **1q** and **1r** still showed moderate effects (IC_{50} = 19–29 µM), **1m** and **1o** achieved values below 10 µM (IC_{50} = 8 µM and 7 µM, respectively). Especially, compounds **1i** and **1j** (IC_{50} = 3.8 µM and 3.2 µM, respectively) demonstrated a remarkable ten-fold enhancement in activity compared to **1a**, and a three-fold increase compared to the reference thiamidol (IC_{50} = 10 µM). 14-days exposure yielded improved melanogenesis suppression, at the expense of increased cytotoxicity, especially for **1j** and thiamidol (CC_{50} = 29 µM and 36 µM, respectively). A similar hierarchy in overall performance was maintained among the tested compounds: **1i** and **1j** reached submicromolar inhibition values, comparable to thiamidol (IC_{50} = 0.53 µM, 0.77 µM and 0.28 µM, respectively), while the remaining derivatives were significantly less potent (IC_{50} = 2.0–12 µM). Importantly, kojic acid was found to be almost inactive in all cases.

Table 2. Structures and activities of indanone derivatives 1a, 1c, 1i, 1j, 1l–o, 1q and 1r in human melanoma MNT-1 whole cells melanogenesis inhibition and cytotoxicity assays at 4 days and 14 days.

compound	R	MNT-1 whole cells (4 d)		MNT-1 whole cells (14 d)	
		melanogenesis IC_{50} (μM)	cytotoxicity CC_{50} (μM)	melanogenesis IC_{50} (μM)	cytotoxicity CC_{50} (μM)
1a	OH	29 ± 2[19]	91 ± 2[19]	—	—
1c	Me	21 ± 2	>100	4.1 ± 0.3	61 ± 2
1i	NH_2	3.8 ± 0.8	>100	0.53 ± 0.06	66 ± 2
1j	NHMe	3.2 ± 0.5	78 ± 6	0.77 ± 0.08	29 ± 1
1l	NHAc	19 ± 2	>100	3.3 ± 0.5	67 ± 2
1m	NHCOEt	8 ± 1	>100	3.1 ± 0.3	65 ± 3
1n	NHCOPr	24 ± 3	>100	2.0 ± 0.2	77 ± 4
1o	NHCO*i*-Pr	7 ± 1	>100	2.1 ± 0.3	62 ± 2
1q	NH-Gly	29 ± 3	>100	12 ± 2	>100
1r	NH-L-Ala	19 ± 2	>100	4.6 ± 0.8	94 ± 7
Kojic acid	—	14000 ± 1000	22000 ± 1000	800 ± 60	2200 ± 80
Thiamidol	—	10 ± 1	>100	0.28 ± 0.01	36.0 ± 0.9

CONCLUSION

In conclusion, we investigated the inhibitory potential of eighteen novel compounds, based on the indanone scaffold, against mushroom and human tyrosinase, as well as their ability to suppress melanin biosynthesis in whole-cell experiments. Among the various chemical groups introduced at position 4, which was previously identified as a critical site for interacting with TYR hot spot residues, amino and amido moieties yielded the best results, both in cell-free and in whole-cell contexts. Specifically, compound **1l** displayed excellent activity against *ab*TYR and *hs*TYR (IC_{50} = 8.6 nM and 140 nM), while compound **1j** effectively inhibited melanin production in melanoma cells (IC_{50} = 0.77 μM in the 14-day experiment), matching thiamidol

potency, a marketed reference inhibitor of *hs*TYR. The recorded effects were further elucidated by molecular docking experiments, demonstrating that compounds **1l**, **1m** and **1n** adopted credible and consistent geometries enabling a strong interaction pattern with TYR active site. In summary, our findings shed light on the potential of this new generation of compounds for TYR-targeting human-directed applications.

EXPERIMENTAL SECTION

Chemistry. ^{1}H and ^{13}C NMR spectra were recorded on an Avance NEO instrument (Bruker, 400 MHz for ^{1}H, 100 MHz for ^{13}C). Chemical shifts are calibrated in ppm relative to the solvent in which the spectrum was recorded. Electrospray ionization (ESI) high resolution mass spectra were acquired at the ICMG PSM Platform on a LTQ Orbitrap XL Thermo Scientific. HPLC analyses were recorded on an Agilent 1260 Infinity II series using a diode array detector and a C18 reversed-phase column (Zorbax Eclipse Plus, Agilent, 3.5 µm particle size, 100 mm × 2.1 mm) at 25 °C, with a mobile phase A composed of water and TFA 0.1% and a phase mobile B composed of MeCN and TFA 0.1% with a gradient 95:5 to 0:100 A:B over 15 min, 1 mL/min, 30 µL injection, detection at 254 nm. Purity of all the tested compounds was ≥95%. Silica gel UV_{254} plates (0.20 mm, Macherey-Nagel) were used for thin-layer chromatography (TLC), and silica gel 60 M (0.015–0.04 mm or 0.04–0.063 mm, Macherey-Nagel) was used for flash chromatography and dry column vacuum chromatography. Unless otherwise stated, solvents and reagents (including kojic acid, thiamidol, **2b** and **2e**–**h**) were obtained from commercial sources (mostly from Sigma, Alfa Aesar, Fluorochem, BLDPharm, VWR) and were used without further purification.

4-Methyl-2,3-dihydro-1*H*-inden-1-one (2c). A solution of 3-*o*-tolylpropanoic acid (197 mg, 1.2 mmol) in trifluoromethanesulfonic acid (0.6 mL) was stirred at 25 °C for 16 h. H_2O (3 mL)

was then added and the mixture was extracted three times with CH_2Cl_2. The combined organic layers were dried over $MgSO_4$, filtered, and the filtrate was concentrated under reduced pressure. The residue was purified by column chromatography on silica gel (eluent cyclohexane / EtOAc) to afford **2c** (159 mg, 89%) as a white solid. ^{1}H NMR (400 MHz, $CDCl_3$) δ 7.61 (d, J = 7.5 Hz, 1H), 7.40 (d, J = 7.5 Hz, 1H), 7.30 (t, J = 7.5 Hz, 1H), 3.06–3.00 (m, 2H), 2.74–2.68 (m, 2H), 2.36 (s, 3H). ^{13}C NMR (100 MHz, $CDCl_3$) δ 207.5, 154.2, 136.9, 135.9, 135.1, 127.5, 121.2, 36.3, 24.7, 17.8. HRMS (ESI) *m/z* calc. for $C_{10}H_{11}O$ $(M+H)^+$: 147.08044. Found: 147.07998.

4-Amino-2,3-dihydro-1*H*-inden-1-one (2i). To a solution of NH_4Cl (722 mg, 13.5 mmol) in EtOH (5.4 mL) and H_2O (5.4 mL) was added iron powder (754 mg, 13.5 mmol), and the suspension was stirred at 60 °C for 30 min. Then, 4-nitro-2,3-dihydro-1*H*-inden-1-one (**2h**, 300 mg, 1.7 mmol) was added, and the suspension was stirred at 80 °C for 45 min. After cooling at 0 °C, an aqueous solution of NaOH (1 M) was added until pH 12. The resulting mixture was filtered, and the filtrate was partially concentrated under reduced pressure. The residue was extracted two times with EtOAc. The combined organic layers were dried over $MgSO_4$, filtered, and the filtrate was concentrated under reduced pressure to afford **2i** (236 mg, 94%) as a brown solid. ^{1}H NMR (400 MHz, d_6-DMSO) δ 7.10 (t, J = 7.6 Hz, 1H), 6.81 (m, 2H), 5.38 (s, 2H), 2.80 (m, 2H), 2.58 (m, 2H). ^{13}C NMR (100 MHz, d_6-DMSO) δ 207.1, 146.3, 139.9, 137.3, 128.1, 117.5, 109.8, 35.7, 22.8. HRMS (ESI) *m/z* calc. for $C_9H_{10}NO$ $(M+H)^+$: 148.07569. Found: 148.07515.

***tert*-Butyl (1-oxo-2,3-dihydro-1*H*-inden-4-yl)carbamate (Boc-2i).** To a solution of **2i** (252 mg, 1.71 mmol) in MeOH (14 mL) was added Boc_2O (446 mg, 2.04 mmol), and the mixture was refluxed for 6 h. After cooling, the mixture was concentrated under reduced pressure to afford Boc-**2i** (159 mg, 38%) as a yellow solid. ^{1}H NMR (400 MHz, d_6-DMSO) δ 9.06 (s, 1H), 7.84 (dd, J = 7.0 Hz, 2.0 Hz, 1H), 7.41–7.31 (m, 2H), 3.07–2.99 (m, 2H), 2.65–2.58 (m, 2H),

1.49 (s, 9H). ^{13}C NMR (100 MHz, d_6-DMSO) δ 206.3, 153.1, 146.8, 137.6, 136.8, 127.8, 126.9, 117.9, 79.5, 35.7, 28.1, 23.4. HRMS (ESI) *m/z* calc. for $C_{14}H_{18}NO_3$ $(M+H)^+$: 248.12812. Found: 248.12854.

***tert*-Butyl methyl(1-oxo-2,3-dihydro-1*H*-inden-4-yl)carbamate (Boc-2j).** To a solution of Boc-**2i** (223 mg, 0.903 mmol) in DMF (4 mL) was added NaH (33 mg, 1.38 mmol) at 0 °C and the mixture was stirred for 20 min. MeI (67 µL, 1.08 mmol) was then added and the mixture was stirred at 25 °C for 16 h. The mixture was extracted two times with Et_2O. The combined organic layers were dried over $MgSO_4$, filtered, and the filtrate was concentrated under reduced pressure. The residue was purified by column chromatography on silica gel (eluent cyclohexane / EtOAc) to afford Boc-**2j** (115 mg, 49%) as a yellow oil. ^{1}H NMR (400 MHz, $CDCl_3$) δ 7.66 (d, J = 6.9 Hz, 1H), 7.39 (m, 2H), 3.23 (s, 3H), 3.04 (m, 2H), 2.70 (m, 2H), 1.41 (s, 9H). ^{13}C NMR (100 MHz, $CDCl_3$) δ 206.8, 154.5, 142.1, 138.6, 132.7, 128.6, 124.6, 122.4, 80.7, 37.1, 36.2, 28.5, 24.0. HRMS (ESI) *m/z* calc. for $C_{15}H_{20}NO_3$ $(M+H)^+$: 262.14377. Found: 262.14412.

4-(Dimethylamino)-2,3-dihydro-1*H*-inden-1-one (2k). To a solution of formaldehyde (0.22 mL, 37%, 2.71 mmol) and aqueous sulfuric acid (0.46 mL, 3 M, 1.36 mmol) was added slowly a solution of **2i** (200 mg, 1.36 mmol) and $NaBH_4$ (186 mg, 4.92 mmol) in THF (5 mL) at 0 °C. The solution was maintained below pH 4 by adding sulfuric acid. The mixture was stirred at 0 °C for 4 h, then aqueous KOH (50%) was added until pH 6. The mixture was extracted two times with PhMe. The combined organic layers were dried over $MgSO_4$, filtered, and the filtrate was concentrated under reduced pressure to afford **2k** as an orange oil (200 mg, 81%). ^{1}H NMR (400 MHz, MeOD) δ 7.33 (t, J = 7.6 Hz, 1H), 7.27 (dd, J = 7.6 Hz, 1.1 Hz, 1H), 7.18 (dd, J = 7.6 Hz, 1.1 Hz, 1H), 3.16 (m, 2H), 2.87 (s, 6H), 2.68 (m, 2H). ^{13}C NMR (100 MHz, MeOD) δ 210.4, 152.9, 149.1, 139.4, 129.6, 123.3, 116.8, 43.3, 37.2, 26.4. HRMS (ESI) *m/z* calc. for $C_{11}H_{14}NO$ $(M+H)^+$: 176.10699. Found: 176.10674.

General procedure for compounds 2l–p. To a solution of **2i** in EtOAc (6 mL/mmol), an anhydride derivative (2.5 equiv) was added and the mixture was refluxed for 3–16 h. After cooling, the solution was washed with H_2O and brine. The organic layer was dried over $MgSO_4$, filtered, and the filtrate was concentrated under reduced pressure. The residue was purified by column chromatography on silica gel (eluent CH_2Cl_2 / MeOH) to afford the corresponding inden-1-one derivative.

***N*-(1-Oxo-2,3-dihydro-1*H*-inden-4-yl)acetamide (2l).** White solid (95 mg, 71%). ^{1}H NMR (400 MHz, $CDCl_3$) δ 8.13 (d, J = 7.7 Hz, 1H), 7.55 (d, J = 7.7 Hz, 1H), 7.38 (t, J = 7.7 Hz, 1H), 7.30 (br s, 1H), 3.01 (m, 2H), 2.71 (m, 2H), 2.24 (s, 3H). ^{13}C NMR (125 MHz, d_6-DMSO) δ 207.2, 169.6, 147.9, 138.6, 137.5, 128.8, 128.5, 119.5, 36.6, 24.6, 24.6. HRMS (ESI) *m/z* calc. for $C_{11}H_{12}O_2N$ $(M+H)^+$: 190.08626. Found: 190.08595.

***N*-(1-Oxo-2,3-dihydro-1*H*-inden-4-yl)propionamide (2m).** Off-white solid (104 mg, 97%). ^{1}H NMR (400 MHz, $CDCl_3$) δ 8.20 (d, J = 7.6 Hz, 1H), 7.56 (d, J = 7.6 Hz, 1H), 7.40 (t, J = 7.6 Hz, 1H), 7.09 (s, 1H), 3.02 (m, 2H), 2.73 (m, 2H), 2.48 (q, J = 7.5 Hz, 2H), 1.29 (t, J = 7.5 Hz, 3H). ^{13}C NMR (100 MHz, $CDCl_3$) δ 206.1, 172.2, 138.1, 135.7, 128.8, 127.1, 120.1, 36.1, 30.7, 23.3, 9.8. HRMS (ESI) *m/z* calc. for $C_{12}H_{14}NO_2$ $(M+H)^+$: 204.10191. Found: 204.10187.

***N*-(1-Oxo-2,3-dihydro-1*H*-inden-4-yl)butyramide (2n).** Brown solid (76 mg, 97%). ^{1}H NMR (400 MHz, $CDCl_3$) δ 8.19 (d, J = 7.9 Hz, 1H), 7.56 (d, J = 7.6 Hz, 1H), 7.40 (t, J = 7.6 Hz, 1H), 7.08 (s, 1H), 3.01 (m, 2H), 2.77–2.69 (m, 2H), 2.42 (t, J = 7.3 Hz, 2H), 1.80 (sext., J = 7.3 Hz, 2H), 1.04 (t, J = 7.3 Hz, 3H). ^{13}C NMR (100 MHz, $CDCl_3$) δ 206.1, 171.4, 138.1, 135.7, 128.8, 127.2, 120.2, 39.6, 36.1, 23.3, 19.2, 13.9. HRMS (ESI) *m/z* calc. for $C_{13}H_{16}NO_2$ $(M+H)^+$: 218.11756. Found: 218.11792.

***N*-(1-Oxo-2,3-dihydro-1*H*-inden-4-yl)isobutyramide (2o).** Off-white solid (308 mg, 89%). ^{1}H NMR (400 MHz, $CDCl_3$) δ 8.21 (d, J = 7.7 Hz, 1H), 7.57 (d, J = 7.7 Hz, 1H), 7.41 (t, J =

7.7 Hz, 1H), 7.07 (s, 1H), 3.02 (m, 2H), 2.75 (m, 2H), 2.61 (hept., J = 6.9 Hz, 1H), 1.31 (d, J = 6.9 Hz, 6H). ^{13}C NMR (100 MHz, $CDCl_3$) δ 206.2, 175.4, 167.8, 138.0, 135.7, 128.8, 127.1, 120.1, 36.7, 36.0, 23.2, 19.8. HRMS (ESI) *m/z* calc. for $C_{13}H_{16}NO_2$ $(M+H)^+$: 218.11756. Found: 218.11718.

***N*-(1-Oxo-2,3-dihydro-1*H*-inden-4-yl)benzamide (2p).** Off-white solid (170 mg, 52%). ^{1}H NMR (400 MHz, $CDCl_3$) δ 8.29 (d, J = 7.6 Hz, 1H), 7.94–7.87 (m, 2H), 7.79 (s, 1H), 7.61 (t, J = 7.6 Hz, 2H), 7.53 (t, J = 7.6 Hz, 2H), 7.46 (t, J = 7.6 Hz, 1H), 3.15–3.06 (m, 2H), 2.81–2.71 (m, 2H). ^{13}C NMR (100 MHz, $CDCl_3$) δ 206.0, 165.7, 145.6, 138.1, 135.6, 134.4, 132.4, 129.1, 128.8, 127.2, 120.4, 36.0, 23.3. HRMS (ESI) *m/z* calc. for $C_{16}H_{14}NO_2$ $(M+H)^+$: 252.10191. Found: 252.10232.

General procedure for compounds 3c–g, 3i, 3l–p. To a solution of a 4-substituted inden-1*H*-one in MeOH (15 mL/mmol) were added NaH (2 equiv) and 2,4-dimethoxybenzaldehyde (1 equiv), and the mixture was stirred at 25 °C for 16 h. Then, the precipitate was filtered, washed with water and dried to afford the corresponding indanone derivative.

(*E*)-2-(2,4-Dimethoxybenzylidene)-4-methyl-2,3-dihydro-1*H*-inden-1-one (3c). Yellow solid (34 mg, 52%). ^{1}H NMR (400 MHz, $CDCl_3$) δ 8.12 (s, 1H), 7.75 (d, J = 7.4 Hz, 1H), 7.70 (d, J = 8.6 Hz, 1H), 7.40 (d, J = 7.4 Hz, 1H), 7.33 (t, J = 7.4 Hz, 1H), 6.61 (dd, J = 8.6 Hz, 2.3 Hz, 1H), 6.50 (d, J = 2.3 Hz, 1H), 3.89 (s, 3H), 3.88 (s, 3H), 3.84 (s, 2H), 2.43 (s, 3H). ^{13}C NMR (100 MHz, $CDCl_3$) δ 194.8, 162.6, 160.9, 148.7, 138.4, 135.2, 134.8, 132.5, 130.9, 128.3, 127.7, 121.8, 117.8, 105.4, 98.5, 55.8, 55.6, 31.5, 18.1. HRMS (ESI) *m/z* calc. for $C_{19}H_{19}O_3$ $(M+H)^+$: 295.13287. Found: 295.13221.

(*E*)-4-Fluoro-2-(2,4-Dimethoxybenzylidene)-2,3-dihydro-1*H*-inden-1-one (3d). Yellow solid (386 mg, 65%). ^{1}H NMR (400 MHz, d_6-DMSO) δ 7.92 (t, J = 1.7 Hz, 1H), 7.79 (d, J = 8.4 Hz, 1H), 7.63 (m, 1H), 7.54 (m, 2H), 6.70 (m, 2H), 4.07 (d, J = 1.7 Hz, 2H), 3.91 (s, 3H),

3.86 (s, 3H). ^{13}C NMR (100 MHz, d_6-DMSO) δ 192.1 (d, J = 2.9 Hz), 162.8, 160.5, 159.3 (d, J = 247.7 Hz), 140.6 (d, J = 5.5 Hz), 135.4 (d, J = 19.6 Hz), 131.1, 130.7, 129.9 (J = 6.9 Hz), 128.0, 120.6, (J = 18.6 Hz), 119.6 (J = 3.9 Hz), 115.8, 106.4, 98.4, 55.9, 55.6, 27.9. HRMS (ESI) *m/z* calc. for $C_{18}H_{16}FO_3$ $(M+H)^+$: 299.10780. Found: 299.10728.

(*E*)-4-Bromo-2-(2,4-Dimethoxybenzylidene)-2,3-dihydro-1*H*-inden-1-one (3e). Yellow solid (170 mg, 89%). ^{1}H NMR (400 MHz, $CDCl_3$) δ 8.16 (s, 1H), 7.85 (d, J = 7.7 Hz, 1H), 7.75 (d, J = 7.7 Hz, 1H), 7.70 (d, J = 8.7 Hz, 1H), 7.32 (t, J = 7.7 Hz, 1H), 6.63 (dd, J = 8.7 Hz, 2.3 Hz, 1H), 6.50 (d, J = 2.3 Hz, 1H), 3.90–3.88 (m, 8H). ^{13}C NMR (100 MHz, $CDCl_3$) δ 193.7, 163.0, 161.1, 149.6, 140.8, 136.9, 131.3, 131.2, 129.6, 129.4, 123.2, 121.7, 117.4, 105.5, 98.6, 55.8, 55.7, 33.9. HRMS (ESI) *m/z* calc. for $C_{18}H_{16}BrO_3$ $(M+H)^+$: 359.02773. Found: 359.02780.

(*E*)-2-(2,4-Dimethoxybenzylidene)-4-trifluoromethyl-2,3-dihydro-1*H*-inden-1-one (3f). Yellow solid (152 mg, 85%). ^{1}H NMR (400 MHz, $CDCl_3$) δ 8.18 (s, 1H), 8.08 (d, J = 7.6 Hz, 1H), 7.85 (d, J = 7.6 Hz, 1H), 7.67 (d, J = 8.6 Hz, 1H), 7.55 (t, J = 7.6 Hz, 1H), 6.63 (dd, J = 8.6 Hz, 2.1 Hz, 1H), 6.50 (d, J = 2.1 Hz, 1H), 4.13 (s, 2H), 3.90 (s, 3H), 3.88 (s, 3H). ^{13}C NMR (100 MHz, d_6-DMSO) δ 191.8, 163.0, 160.6, 146.7, 139.3, 131.2, 131.1 (q, J = 4.4 Hz), 130.4, 128.7, 128.3, 127.7, 126.6 (q, J = 31.8 Hz), 124.1 (q, J = 273.5 Hz), 115.9, 106.5, 98.5, 56.0, 55.6, 30.9. HRMS (ESI) *m/z* calc. for $C_{19}H_{16}F_3O_3$ $(M+H)^+$: 349.10461. Found: 349.10433.

(*E*)-2-(2,4-Dimethoxybenzylidene)-1-oxo-2,3-dihydro-1*H*-indene-4-carbonitrile (3g). Green solid (180 mg, 89%). ^{1}H NMR (400 MHz, $CDCl_3$) δ 8.21 (s, 1H), 8.11 (d, J = 7.6 Hz, 1H), 7.88 (d, J = 7.6 Hz, 1H), 7.68 (d, J = 8.7 Hz, 1H), 7.55 (t, J = 7.6 Hz, 1H), 6.63 (dd, J = 8.7 Hz, 2.2 Hz, 1H), 6.50 (d, J = 2.2 Hz, 1H), 4.13 (s, 2H), 3.90 (s, 3H), 3.89 (s, 3H). ^{13}C NMR (100 MHz, $CDCl_3$) δ 192.3, 163.4, 161.2, 152.7, 139.8, 136.9, 131.4, 130.8, 129.8, 128.6, 128.4, 117.0, 116.7, 110.8, 105.7, 98.7, 55.8, 55.7, 32.2. HRMS (ESI) *m/z* calc. for $C_{19}H_{16}NO_3$ $(M+H)^+$: 306.11247. Found: 306.11229.

(*E*)-4-Amino-2-(2,4-dimethoxybenzylidene)-2,3-dihydro-1*H*-inden-1-one (3i). Yellow solid (82 mg, 75%). ^{1}H NMR (400 MHz, d_6-DMSO) δ 7.82 (m, 2H), 7.15 (t, J = 7.7 Hz, 1H), 6.95 (d, J = 7.4 Hz, 1H), 6.84 (d, J = 7.7 Hz, 1H), 6.67 (m, 2H), 5.48 (s, 2H), 3.91 (s, 3H), 3.86 (s, 3H), 3.73 (s, 2H). ^{13}C NMR (100 MHz, d_6-DMSO) δ 194.0, 162.3, 160.3, 145.9, 138.1, 134.1, 132.2, 130.6, 128.4, 125.9, 117.9, 116.3, 110.5, 106.2, 98.3, 55.9, 55.5, 29.7. HRMS (ESI) *m/z* calc. for $C_{18}H_{18}NO_3$ $(M+H)^+$: 296.12812. Found: 296.12782.

(*E*)-*N*-(2-(2,4-Dimethoxybenzylidene)-1-oxo-2,3-dihydro-1*H*-inden-4-yl)acetamide (3l). Yellow solid (20 mg, 57%). ^{1}H NMR (400 MHz, d_6-DMSO) δ 9.67 (s, 1H), 8.10 (d, J = 7.5 Hz, 1H), 7.88 (s, 1H), 7.79 (d, J = 8.4 Hz, 1H), 7.51 (d, J = 7.5 Hz, 1H), 7.43 (t, J = 7.5 Hz, 1H), 6.71 (m, 2H), 3.98 (s, 2H), 3.91 (s, 3H), 3.87 (s, 3H), 2.18 (s, 2H). ^{13}C NMR (100 MHz, d_6-DMSO) δ 193.1, 168.7, 162.6, 160.5, 140.8, 139.4, 136.2, 131.4, 130.7, 128.1, 127.0, 126.7, 118.9, 116.1, 106.3, 98.4, 55.9, 55.6, 30.2, 23.8. HRMS (ESI) *m/z* calc. for $C_{20}H_{20}NO_4$ $(M+H)^+$: 338.13868. Found: 338.13831.

(*E*)-*N*-(2-(2,4-Dimethoxybenzylidene)-1-oxo-2,3-dihydro-1*H*-inden-4-yl)propionamide (3m). Yellow solid (129 mg, 73%). ^{1}H NMR (400 MHz, d_6-DMSO) δ 9.58 (s, 1H), 8.12 (d, J = 7.6 Hz, 1H), 7.88 (s, 1H), 7.79 (d, J = 8.5 Hz, 1H), 7.51 (d, J = 7.6 Hz, 1H), 7.43 (t, J = 7.6 Hz, 1H), 6.72 (m, 2H), 3.98 (s, 2H), 3.91 (s, 3H), 3.87 (s, 3H), 2.48 (q, J = 7.5 Hz, 2H), 1.15 (t, J = 7.5 Hz, 3H). ^{13}C NMR (100 MHz, d_6-DMSO) δ 193.0, 172.4, 162.5, 160.4, 138.4, 136.1, 131.5, 130.6, 128.0, 127.0, 127.0, 126.7, 118.8, 116.1, 106.3, 98.4, 55.9, 55.5, 30.1, 29.1, 9.7. HRMS (ESI) *m/z* calc. for $C_{21}H_{22}NO_4$ $(M+H)^+$: 352.15433. Found: 352.15378.

(*E*)-*N*-(2-(2,4-Dimethoxybenzylidene)-1-oxo-2,3-dihydro-1*H*-inden-4-yl)butyramide (3n). Yellow solid (361 mg, 76%). ^{1}H NMR (400 MHz, d_6-DMSO) δ 9.61 (s, 1H), 8.09 (d, J = 7.4 Hz, 1H), 7.88 (s, 1H), 7.77 (d, J = 8.3 Hz, 1H), 7.52 (d, J = 7.4 Hz, 1H), 7.44 (t, J = 7.4 Hz, 1H), 6.71 (m, 2H), 3.97 (s, 2H), 3.91 (s, 3H), 3.87 (s, 3H), 2.44 (m, 2H), 1.67 (m, 2H), 0.98 (t, J = 7.1 Hz, 3H). ^{13}C NMR (100 MHz, d_6-DMSO) δ 193.1, 171.5, 162.6, 160.5, 141.1, 138.4,

136.1, 131.5, 130.6, 128.1, 127.2, 126.7, 118.9, 116.1, 106.3, 98.4, 55.9, 55.6, 37.9, 30.3, 18.6, 13.6. HRMS (ESI) *m/z* calc. for $C_{22}H_{24}NO_4$ $(M+H)^+$: 365.16998. Found: 365.17016.

(*E*)-*N*-(2-(2,4-Dimethoxybenzylidene)-1-oxo-2,3-dihydro-1*H*-inden-4-yl)isobutyramide (3o). Yellow solid (370 mg, 72%). ^{1}H NMR (400 MHz, d_6-DMSO) δ 9.56 (s, 1H), 8.07 (d, J = 7.6 Hz, 1H), 7.88 (s, 1H), 7.78 (d, J = 8.5 Hz, 1H), 7.52 (d, J = 7.6 Hz, 1H), 7.44 (t, J = 7.6 Hz, 1H), 6.75–6.67 (m, 2H), 3.98 (s, 2H), 3.91 (s, 3H), 3.87 (s, 3H), 2.81 (hept., J = 6.8 Hz, 1H), 1.17 (d, J = 6.8 Hz, 6H). ^{13}C NMR (100 MHz, d_6-DMSO) δ 193.1, 175.7, 162.6, 160.5, 141.3, 138.4, 136.2, 131.5, 130.7, 128.1, 127.3, 126.8, 119.0, 116.2, 106.3, 98.4, 55.9, 55.6, 34.5, 30.2, 19.6. HRMS (ESI) *m/z* calc. for $C_{22}H_{24}NO_4$ $(M+H)^+$: 366.16998. Found: 366.17044.

(*E*)-*N*-(2-(2,4-Dimethoxybenzylidene)-1-oxo-2,3-dihydro-1*H*-inden-4-yl)benzamide (3p). Green solid (258 mg, 92%). ^{1}H NMR (400 MHz, d_6-DMSO) δ 10.23 (s, 1H), 8.03 (d, J = 7.3 Hz, 2H), 7.92 (d, J = 7.8 Hz, 1H), 7.90 (s, 1H), 7.72 (d, J = 9.1 Hz, 1H), 7.64 (m, 2H), 7.58 (t, J = 7.3 Hz, 2H), 7.52 (t, J = 7.3 Hz, 1H), 6.68 (m, 2H), 4.07 (s, 2H), 3.90 (s, 3H), 3.83 (s, 3H). ^{13}C NMR (100 MHz, d_6-DMSO) δ 193.1, 165.7, 162.6, 160.4, 143.4, 138.6, 136.0, 134.4, 131.9, 131.5, 130.7, 129.6, 128.5, 128.1, 128.0, 126.9, 120.2, 116.1, 106.3, 98.5, 55.9, 55.5, 30.5. HRMS (ESI) *m/z* calc. for $C_{25}H_{22}NO_4$ $(M+H)^+$: 400.15433. Found: 400.15465.

General procedure for compounds Boc-3q–s. To a solution of a Boc-protected amino acid (1.4 equiv) in CH_2Cl_2 (18 mL/mmol) were added HOBt (1 equiv) and DCC (1.7 equiv) at 0 °C, and the mixture was stirred at 25 °C for 35 min. Then, **2i** was added and the mixture was stirred at 25 °C for 16 h. The solution was concentrated under reduced pressure. Et_2O was added to the residue, and after filtration the solution was washed with saturated $NaHCO_3$, H_2O and brine. The organic layer was dried over $MgSO_4$, filtered, and the filtrate was concentrated under reduced pressure. The residue was purified by column chromatography on silica gel (eluent CH_2Cl_2 / MeOH). To a solution of the crude 4-substituted inden-1-one derivative in MeOH (15 mL/mmol) were added NaH (2 equiv) and 2,4-dimethoxybenzaldehyde (1 equiv), and the

mixture was stirred at 25 °C for 16 h. Then, the precipitate was filtered, washed with water and dried to afford the corresponding indanone derivative.

***tert*-Butyl (*E*)-(2-((2-(2,4-dimethoxybenzylidene)-1-oxo-2,3-dihydro-1*H*-inden-4-yl)amino)-2-oxoethyl)carbamate (Boc-3q).** Yellow solid (177 mg, 74%). ^{1}H NMR (400 MHz, d_6-DMSO) δ 9.69 (s, 1H), 8.07 (d, J = 7.6 Hz, 1H), 7.89 (s, 1H), 7.79 (d, J = 8.8 Hz, 1H), 7.54 (d, J = 7.6 Hz, 1H), 7.45 (t, J = 7.6 Hz, 1H), 7.14 (t, J = 5.9 Hz, 1H), 6.68 (m, 2H), 3.96 (s, 2H), 3.91 (s, 3H), 3.86 (m, 5H), 1.41 (s, 9H). ^{13}C NMR (100 MHz, d_6-DMSO) δ 193.1, 168.8, 162.6, 160.5, 156.1, 141.1, 138.5, 135.9, 131.4, 130.7, 128.2, 127.1, 126.8, 119.2, 116.1, 106.3, 98.4, 78.2, 56.0, 55.6, 43.8, 30.2, 28.2. HRMS (ESI) *m/z* calc. for $C_{25}H_{29}N_2O_6$ $(M+H)^+$: 453.20201. Found: 453.20211.

***tert*-Butyl (*S*,*E*)-(1-((2-(2,4-dimethoxybenzylidene)-1-oxo-2,3-dihydro-1*H*-inden-4-yl)amino)-1-oxopropan-2-yl)carbamate (Boc-3r).** Yellow solid (180 mg, 43%). ^{1}H NMR (400 MHz, d_6-DMSO) δ 9.69 (s, 1H), 8.02 (d, J = 7.5 Hz, 1H), 7.89 (s, 1H), 7.78 (d, J = 8.4 Hz, 1H), 7.55 (d, J = 7.5 Hz, 1H), 7.46 (t, J = 7.5 Hz, 1H), 7.19 (d, J = 7.1 Hz, 1H), 6.68 (m, 2H), 4.29 (quint., J = 7.1 Hz, 1H), 3.95 (s, 2H), 3.92 (s, 3H), 3.86 (s, 3H), 1.40 (s, 9H), 1.35 (d, J = 7.1 Hz, 3H). ^{13}C NMR (100 MHz, d_6-DMSO) δ 193.0, 172.3, 162.6, 160.5, 155.4, 141.5, 138.5, 135.9, 131.4, 130.6, 128.2, 127.4, 126.8, 119.3, 116.1, 106.3, 98.4, 78.2, 55.9, 55.6, 50.3, 30.2, 28.2, 18.0. HRMS (ESI) *m/z* calc. for $C_{26}H_{31}N_2O_6$ $(M+H)^+$: 467.21766. Found: 467.21767.

***tert*-Butyl (*S*,*E*)-(1-((2-(2,4-dimethoxybenzylidene)-1-oxo-2,3-dihydro-1*H*-inden-4-yl)amino)-3-methyl-1-oxobutan-2-yl)carbamate (Boc-3s).** Yellow solid (105 mg, 83%). ^{1}H NMR (400 MHz, $CDCl_3$) δ 8.35 (s, 1H), 8.21 (d, J = 7.7 Hz, 1H), 8.12 (s, 1H), 7.70 (m, 2H), 7.42 (t, J = 7.7 Hz, 1H), 6.57 (dd, J = 8.7 Hz, 2.3 Hz, 1H), 6.49 (d, J = 2.3 Hz, 1H), 5.15 (d, J = 8.0 Hz, 1H), 4.03 (t, J = 8.0 Hz, 1H), 3.88 (s, 3H), 3.86 (m, 5H), 2.36 (oct., J = 6.7 Hz, 1H), 1.46 (s, 9H), 1.09 (d, J = 6.7 Hz, 3H), 1.06 (d, J = 6.7 Hz, 3H). ^{13}C NMR (100 MHz, d_6-DMSO) δ 193.0, 171.0, 162.6, 160.5, 155.8, 141.8, 138.5, 135.7, 131.4, 130.5, 128.2, 127.8, 126.8,

119.5, 116.1, 106.2, 98.5, 78.1, 60.2, 55.9, 55.6, 30.5, 30.2, 28.2, 19.3, 18.4. HRMS (ESI) *m/z* calc. for $C_{28}H_{35}N_2O_6$ $(M+H)^+$: 495.24896. Found: 495.24705.

General procedure for compounds 1c–g, 1i, 1l–s. To a solution of a 2',4'-dimethoxyindanone derivative in dry CH_2Cl_2 (10 mL/mmol) was added a solution of BBr_3 in CH_2Cl_2 (1 M, 10–20 equiv) at 0 °C, and the mixture was stirred at 25 °C for 24–96 h. Iced water was then added and the suspension was stirred at 25 °C for 1 h. The mixture was extracted three times with EtOAc. The combined organic layers were dried over $MgSO_4$, filtered, and the filtrate was concentrated under reduced pressure. The residue was purified by column chromatography on silica gel (eluent CH_2Cl_2 / MeOH) to afford the corresponding 2',4'-dihydroxyindanone.

(*E*)-2-(2,4-Dihydroxybenzylidene)-4-methyl-2,3-dihydro-1*H*-inden-1-one (1c). Yellow solid (20 mg, 28%). ^{1}H NMR (400 MHz, MeOD) δ 8.15 (s, 1H), 7.67 (d, J = 8.6 Hz, 1H), 7.63 (d, J = 7.5 Hz, 1H), 7.46 (d, J = 7.5 Hz, 1H), 7.34 (t, J = 7.5 Hz, 1H), 6.44 (dd, J = 8.6 Hz, 2.4 Hz, 1H), 6.37 (d, J = 2.4 Hz, 1H), 3.88 (s, 2H), 2.45 (s, 3H). ^{13}C NMR (100 MHz, MeOD) δ 197.3, 162.7, 161.4, 150.5, 139.2, 136.9, 136.1, 132.4, 131.3, 131.2, 128.8, 122.1, 115.8, 109.1, 103.5, 32.3, 17.9. HRMS (ESI) *m/z* calc. for $C_{17}H_{13}O_3$ $(M-H)^-$: 265.08702. Found: 265.08659.

(*E*)-4-Fluoro-2-(2,4-dihydroxybenzylidene)-2,3-dihydro-1*H*-inden-1-one (1d). Yellow solid (20 mg, 15%). ^{1}H NMR (400 MHz, d_6-DMSO) δ 10.24 (s, 1H), 10.03 (s, 1H), 7.96 (t, J = 1.5 Hz, 1H), 7.61 (m, 2H), 7.51 (m, 2H), 6.41 (m, 2H), 4.02 (d, J = 1.5 Hz, 2H). ^{13}C NMR (100 MHz, d_6-DMSO) δ 192.0 (d, J = 2.9 Hz), 161.3, 159.9, 159.4 (d, J = 247.8 Hz), 141.0 (d, J = 5.2 Hz), 135.2 (d, J = 18.5 Hz), 131.2, 129.8 (d, J = 6.3 Hz), 129.3, 128.3, 120.3 (d, J = 19.2 Hz), 119.5 (d, J = 3.8 Hz), 113.3, 108.2, 102.4, 28.1. HRMS (ESI) *m/z* calc. for $C_{16}H_{12}FO_3$ $(M+H)^+$: 271.07650. Found: 271.07640.

(*E*)-4-Bromo-2-(2,4-dihydroxybenzylidene)-2,3-dihydro-1*H*-inden-1-one (1e). Yellow solid (58 mg, 45%). ^{1}H NMR (400 MHz, d_6-DMSO) δ 10.25 (s, 1H), 10.05 (s, 1H), 7.97 (s,

1H), 7.91 (d, *J* = 7.5 Hz, 1H), 7.76 (d, *J* = 7.5 Hz, 1H), 7.60 (d, *J* = 9.3 Hz, 1H), 7.44 (t, *J* = 7.5 Hz, 1H), 6.44 (m, 2H), 3.90 (s, 2H). ^{13}C NMR (100 MHz, d_6-DMSO) δ 192.4, 161.4, 160.0, 149.2, 140.2, 136.7, 131.1, 129.8, 129.2, 128.6, 122.5, 121.2, 113.4, 108.2, 102.5, 33.2. HRMS (ESI) *m/z* calc. for $C_{16}H_{10}BrO_3$ $(M–H)^-$: 328.98188. Found: 328.98135.

(*E*)-2-(2,4-Dihydroxybenzylidene)-4-(trifluoromethyl)-2,3-dihydro-1*H*-inden-1-one (1f). Yellow solid (65 mg, 53%). ^{1}H NMR (400 MHz, d_6-DMSO) δ 10.27 (s, 1H), 10.07 (s, 1H), 8.03 (m, 2H), 7.99 (s, 1H), 7.70 (t, *J* = 7.7 Hz, 1H), 7.57 (d, *J* = 9.3 Hz, 1H), 6.44 (m, 2H), 4.13 (s, 2H). ^{13}C NMR (100 MHz, d_6-DMSO) δ 191.6, 161.5, 160.0, 146.4, 139.6, 131.2, 130.7 (q, *J* = 4.6 Hz), 129.5, 128.5, 127.9, 127.4, 126.5 (q, *J* = 31.7 Hz), 124.1 (q, *J* = 273.7 Hz), 113.3, 108.3, 102.5, 31.0. HRMS (ESI) *m/z* calc. for $C_{17}H_{10}F_3O_3$ $(M–H)^-$: 319.05875. Found: 319.05850.

(*E*)-2-(2,4-Dihydroxybenzylidene)-1-oxo-2,3-dihydro-1*H*-indene-4-carbonitrile (1g). Yellow solid (7 mg, 5%). ^{1}H NMR (400 MHz, MeOD) δ 8.23 (t, *J* = 1.7 Hz, 1H), 8.07 (d, *J* = 7.7 Hz, 1H), 8.01 (dd, *J* = 7.7 Hz, 1.1 Hz, 1H), 7.64 (m, 2H), 6.48 (dd, *J* = 8.5 Hz, 2.3 Hz, 1H), 6.38 (d, *J* = 2.3 Hz, 1H), 4.17 (d, *J* = 1.7 Hz, 2H). ^{13}C NMR (100 MHz, d_6-DMSO) δ 191.5, 161.6, 160.1, 152.7, 138.9, 137.4, 131.2, 129.7, 128.6, 127.9, 127.8, 116.6, 113.3, 110.0, 108.3, 102.4, 31.4. HRMS (ESI) *m/z* calc. for $C_{17}H_{10}NO_3$ $(M–H)^-$: 276.06662. Found: 276.06584.

(*E*)-4-Amino-2-(2,4-dihydroxybenzylidene)-2,3-dihydro-1*H*-inden-1-one (1i). Red solid (11 mg, 16%). ^{1}H NMR (400 MHz, d_6-DMSO) δ 10.13 (s, 1H), 9.93 (s, 1H), 7.86 (s, 1H), 7.66 (d, *J* = 8.6 Hz, 1H), 7.14 (t, *J* = 7.5 Hz, 1H), 6.93 (d, *J* = 7.5 Hz, 1H), 6.82 (d, *J* = 7.5 Hz, 1H), 6.43 (d, *J* = 2.3 Hz, 1H), 6.38 (dd, *J* = 8.6 Hz, 2.3 Hz, 1H), 5.46 (s, 2H), 3.68 (s, 2H). ^{13}C NMR (100 MHz, d_6-DMSO) δ 194.0, 160.7, 159.6, 145.8, 138.4, 134.0, 130.8, 129.9, 128.2, 127.1, 117.6, 113.8, 110.4, 107.8, 102.5, 29.8. HRMS (ESI) *m/z* calc. for $C_{16}H_{14}NO_3$ $(M+H)^+$: 268.09682. Found: 268.09683.

(*E*)-*N*-(2-(2,4-Dihydroxybenzylidene)-1-oxo-2,3-dihydro-1*H*-inden-4-yl)acetamide (1l). Orange solid (23 mg, 25%). ^{1}H NMR (400 MHz, d_6-DMSO) δ 10.19 (br s, 2H), 9.67 (s, 1H), 8.12 (d, J = 7.6 Hz, 1H), 7.92 (s, 1H), 7.64 (d, J = 8.6 Hz, 1H), 7.49 (d, J = 7.6 Hz, 1H), 7.42 (t, J = 7.6 Hz, 1H), 6.45 (d, J = 2.2 Hz, 1H), 6.42 (dd, J = 8.6 Hz, 2.2 Hz, 1H), 3.94 (s, 2H), 2.18 (s, 3H). ^{13}C NMR (100 MHz, d_6-DMSO) δ 193.1, 168.8, 161.2, 160.0, 140.5, 138.7, 136.2, 130.8, 129.0, 128.0, 128.0, 126.5, 118.7, 113.6, 108.0, 102.5, 30.4, 23.8. HRMS (ESI) *m/z* calc. for $C_{18}H_{16}NO_4$ $(M+H)^+$: 310.10738. Found: 310.10756.

(*E*)-*N*-(2-(2,4-Dihydroxybenzylidene)-1-oxo-2,3-dihydro-1*H*-inden-4-yl)propionamide (1m). Orange solid (45 mg, 17%). ^{1}H NMR (400 MHz, d_6-DMSO) δ 10.21 (s, 1H), 10.01 (s, 1H), 9.55 (s, 1H), 8.13 (d, J = 7.6 Hz, 1H), 7.92 (s, 1H), 7.64 (d, J = 8.6 Hz, 1H), 7.49 (d, J = 7.6 Hz, 1H), 7.42 (t, J = 7.6 Hz, 1H), 6.45 (d, J = 2.3 Hz, 1H), 6.42 (dd, J = 8.6 Hz, 2.3 Hz, 1H), 3.93 (s, 2H), 2.49 (q, J = 7.5 Hz, 2H), 1.14 (t, J = 7.5 Hz, 3H). ^{13}C NMR (100 MHz, d_6-DMSO) δ 193.1, 172.5, 161.1, 159.8, 140.5, 138.7, 136.2, 130.8, 129.1, 128.0, 127.9, 126.6, 118.6, 113.6, 108.0, 102.5, 30.3, 29.2, 9.7. HRMS (ESI) *m/z* calc. for $C_{19}H_{18}NO_4$ $(M+H)^+$: 324.12303. Found: 324.12337.

(*E*)-*N*-(2-(2,4-dihydroxybenzylidene)-1-oxo-2,3-dihydro-1*H*-inden-4-yl)butyramide (1n). Yellow solid (50 mg, 15%). ^{1}H NMR (400 MHz, d_6-DMSO) δ 10.20 (s, 1H), 10.00 (s, 1H), 9.58 (s, 1H), 8.09 (d, J = 7.6 Hz, 1H), 7.92 (s, 1H), 7.62 (d, J = 8.6 Hz, 1H), 7.49 (d, J = 7.6 Hz, 1H), 7.42 (t, J = 7.6 Hz, 1H), 6.44 (d, J = 1.9 Hz, 1H), 6.41 (dd, J = 8.6 Hz, 1.9 Hz, 1H), 3.92 (s, 2H), 2.45 (t, J = 7.3 Hz, 2H), 1.68 (sext., J = 7.3 Hz, 2H), 0.98 (t, J = 7.3 Hz, 3H). ^{13}C NMR (100 MHz, MeOD) δ 196.4, 175.0, 162.9, 161.6, 144.1, 140.5, 136.8, 132.4, 131.4, 130.6, 129.8, 129.3, 121.5, 115.7, 109.0, 103.5, 39.3, 31.9, 20.4, 14.1. HRMS (ESI) *m/z* calc. for $C_{20}H_{20}NO_4$ $(M+H)^+$: 338.13868. Found: 338.13861.

(*E*)-*N*-(2-(2,4-Dihydroxybenzylidene)-1-oxo-2,3-dihydro-1*H*-inden-4-yl)isobutyramide (1o). Yellow solid (42 mg, 15%). ^{1}H NMR (400 MHz, d_6-DMSO) δ 10.20 (s, 1H), 10.00 (s,

1H), 9.52 (s, 1H), 8.09 (d, *J* = 7.6 Hz, 1H), 7.91 (s, 1H), 7.63 (d, *J* = 8.6 Hz, 1H), 7.49 (d, *J* = 7.6 Hz, 1H), 7.42 (t, *J* = 7.6 Hz, 1H), 6.42 (m, 2H), 3.93 (s, 2H), 2.82 (hept., *J* = 6.8 Hz, 1H), 1.17 (d, *J* = 6.8 Hz, 6H). ^{13}C NMR (100 MHz, MeOD) δ 196.4, 179.1, 162.9, 161.6, 144.3, 140.5, 136.8, 132.4, 131.5, 130.6, 130.0, 129.3, 121.5, 115.7, 109.1, 103.5, 36.6, 31.8, 20.1. HRMS (ESI) *m/z* calc. for $C_{20}H_{20}NO_4$ $(M+H)^+$: 338.13868. Found: 338.13802.

(*E*)-*N*-(2-(2,4-Dihydroxybenzylidene)-1-oxo-2,3-dihydro-1*H*-inden-4-yl)benzamide (1p). Orange solid (15 mg, 15%). ^{1}H NMR (400 MHz, *d*$_6$-DMSO) δ 10.20 (s, 1H), 10.18 (s, 1H), 9.99 (s, 1H), 8.03 (m, 2H), 7.94 (m, 2H), 7.58 (m, 6H), 6.43 (d, *J* = 2.3 Hz, 1H), 6.37 (dd, *J* = 8.6 Hz, 2.3 Hz, 1H), 4.03 (s, 2H). ^{13}C NMR (100 MHz, *d*$_6$-DMSO) δ 193.1, 165.7, 161.0, 159.8, 143.1, 138.9, 135.9, 134.5, 131.8, 130.8, 129.2, 129.2, 128.5, 128.1, 128.0, 127.9, 120.0, 113.6, 108.0, 102.5, 30.5. HRMS (ESI) *m/z* calc. for $C_{23}H_{18}NO_4$ $(M+H)^+$: 372.12303. Found: 372.12332.

(*E*)-2-Amino-*N*-(2-(2,4-dihydroxybenzylidene)-1-oxo-2,3-dihydro-1*H*-inden-4-yl)acetamide (1q). Yellow solid (7 mg, 6%). ^{1}H NMR (400 MHz, MeOD) δ 8.18 (s, 1H), 8.11 (d, *J* = 7.7 Hz, 1H), 7.72 (d, *J* = 8.7 Hz, 1H), 7.66 (d, *J* = 7.7 Hz, 1H), 7.47 (t, *J* = 7.7 Hz, 1H), 6.45 (dd, *J* = 8.7 Hz, 2.3 Hz, 1H), 6.39 (d, *J* = 2.3 Hz, 1H), 4.05 (s, 2H), 4.01 (s, 2H). ^{13}C NMR (100 MHz, MeOD) δ 196.3, 166.8, 162.9, 161.6, 143.2, 140.6, 136.1, 132.6, 131.6, 130.3, 129.4, 128.8, 121.6, 115.6, 109.2, 103.4, 42.6, 31.9. HRMS (ESI) *m/z* calc. for $C_{18}H_{17}N_2O_4$ $(M+H)^+$: 325.11828. Found: 325.11862.

(*S*,*E*)-2-Amino-*N*-(2-(2,4-dihydroxybenzylidene)-1-oxo-2,3-dihydro-1*H*-inden-4-yl)propenamide (1r). Yellow solid (7 mg, 5%). ^{1}H NMR (400 MHz, MeOD) δ 8.18 (s, 1H), 8.03 (d, *J* = 7.7 Hz, 1H), 7.68 (m, 2H), 7.47 (t, *J* = 7.7 Hz, 1H), 6.43 (dd, *J* = 8.6 Hz, 2.3 Hz, 1H), 6.38 (d, *J* = 2.3 Hz, 1H), 4.11 (q, *J* = 7.0 Hz, 1H), 3.98 (s, 2H), 1.62 (d, *J* = 7.0 Hz, 3H). ^{13}C NMR (100 MHz, MeOD) δ 196.2, 172.9, 163.0, 161.7, 143.7, 140.6, 136.1, 132.4, 131.7,

130.3, 129.4, 129.3, 121.7, 115.6, 109.1, 103.5, 51.3, 31.7, 19.5. HRMS (ESI) *m/z* calc. for $C_{19}H_{19}N_2O_4$ $(M+H)^+$: 339.13393. Found: 339.13417.

(*S*,*E*)-2-Amino-*N*-(2-(2,4-dihydroxybenzylidene)-1-oxo-2,3-dihydro-1*H*-inden-4-yl)-3-methylbutanamide (1s). Red solid (92 mg, 82%). ^{1}H NMR (400 MHz, d_6-DMSO) δ 8.00 (d, J = 7.4 Hz, 1H), 7.93 (s, 1H), 7.60 (d, J = 8.7 Hz, 1H), 7.56 (s, J = 7.4 Hz, 1H), 7.47 (t, J = 7.4 Hz, 1H), 6.46 (d, J = 2.2 Hz, 1H), 6.39 (dd, J = 8.7 Hz, 2.2 Hz, 1H), 3.95 (s, 2H), 3.69 (d, J = 5.3 Hz, 1H), 2.16 (m, 1H), 1.04 (d, J = 6.8 Hz, 3H), 1.00 (d, J = 6.8 Hz, 3H). ^{13}C NMR (100 MHz, d_6-DMSO) δ 192.9, 170.9, 161.2, 159.9, 141.5, 138.9, 135.2, 130.8, 129.0, 128.2, 128.2, 127.1, 119.5, 113.6, 108.0, 102.6, 59.1, 30.9, 30.6, 19.0, 17.5. HRMS (ESI) *m/z* calc. for $C_{21}H_{23}N_2O_4$ $(M+H)^+$: 367.16523. Found: 367.16514.

General procedure for compounds 1b, 1h and 1k. To a solution of a 4-substituted inden-1*H*-one in MeOH (15 mL/mmol) were added $SOCl_2$ (1.5 equiv) dropwise then 2,4-dihydroxybenzaldehyde (1 equiv), and the mixture was stirred at 25 °C for 24–72 h. The mixture was concentrated under reduced pressure, then the residue was purified by column chromatography on silica gel (eluent CH_2Cl_2 / MeOH) to afford the corresponding 2',4'-dihydroxyindanone.

(*E*)-2-(2,4-Dihydroxybenzylidene)-4-methoxy-2,3-dihydro-1*H*-inden-1-one (1b). Yellow solid (22 mg, 2%). ^{1}H NMR (400 MHz, d_6-DMSO) δ 10.16 (s, 1H), 9.97 (s, 1H), 7.90 (s, 1H), 7.59 (d, J = 9.2 Hz, 1H), 7.44 (t, J = 7.7 Hz, 1H), 7.33 (d, J = 7.7 Hz, 1H), 7.26 (d, J = 7.7 Hz, 1H), 6.40 (m, 2H), 3.92 (s, 3H), 3.82 (s, 2H). ^{13}C NMR (100 MHz, d_6-DMSO) δ 193.2, 161.0, 159.7, 156.5, 139.4, 137.6, 131.0, 129.2, 129.2, 128.3, 115.4, 115.0, 113.6, 108.1, 102.4, 55.5, 29.1. HRMS (ESI) *m/z* calc. for $C_{17}H_{13}O_4$ $(M-H)^-$: 281.08193. Found: 281.08187.

(*E*)-2-(2,4-Dihydroxybenzylidene)-4-nitro-2,3-dihydro-1*H*-inden-1-one (1h). Brown solid (19 mg, 6%). ^{1}H NMR (400 MHz, d_6-DMSO) δ 10.31 (s, 1H), 10.12 (s, 1H), 8.50 (dd, J = 7.8 Hz, 0.7 Hz, 1H), 8.17 (dd, J = 7.8 Hz, 0.7 Hz, 1H), 8.00 (s, 1H), 7.77 (t, J = 7.8 Hz, 1H), 7.61

(d, *J* = 8.6 Hz, 1H), 6.46 (m, 2H), 4.41 (s, 2H). ^{13}C NMR (100 MHz, *d*$_6$-DMSO) δ 191.1, 161.6, 160.2, 145.6, 144.3, 140.9, 131.1, 129.7, 129.4, 129.3, 129.2, 128.0, 113.3, 108.3, 102.5, 33.0. HRMS (ESI) *m/z* calc. for $C_{16}H_{10}NO_5$ $(M–H)^-$: 296.05645. Found: 296.05536.

(*E*)-2-(2,4-Dihydroxybenzylidene)-4-(dimethylamino)-2,3-dihydro-1*H*-inden-1-one (1k). Red solid (20 mg, 5%). ^{1}H NMR (400 MHz, *d*$_6$-DMSO) δ 10.33 (s, 2H), 7.97 (s, 1H), 7.91 (m, 1H), 7.74 (d, *J* = 7.7 Hz, 1H), 7.71 (s, *J* = 8.7 Hz, 1H), 7.62 (t, *J* = 7.7 Hz, 1H), 6.49 (d, *J* = 2.3 Hz, 1H), 6.42 (dd, *J* = 8.7 Hz, 2.3 Hz, 1H), 4.30 (s, 2H), 3.20 (s, 6H). ^{13}C NMR (100 MHz, *d*$_6$-DMSO) δ 192.2, 161.6, 160.2, 142.8, 141.5, 140.1, 131.3, 129.5, 128.9, 128.2, 125.2, 122.5, 113.4, 108.3, 102.6, 45.1, 31.3. HRMS (ESI) *m/z* calc. for $C_{18}H_{16}NO_3$ $(M–H)^-$: 294.11357. Found: 294.11332.

(*E*)-2-(2,4-Dihydroxybenzylidene)-4-(methylamino)-2,3-dihydro-1*H*-inden-1-one (1j). To a solution of Boc-**2j** (115 mg, 0.440 mmol) in MeOH (4 mL) were added NaH (21 mg, 0.892 mmol) and 2,4-dimethoxybenzaldehyde (74 mg, 0.440 mmol), and the mixture was stirred at 25 °C for 16 h. Then, the mixture was concentrated under reduced pressure and EtOAc was added. The organic layer was washed three times with H_2O, dried over $MgSO_4$, filtered, and the filtrate was concentrated under reduced pressure. The residue was purified by dry column vacuum chromatography on silica gel (eluent cyclohexane / EtOAc) to afford Boc-**3j**, that was used directly in the next step without further purification and characterization. To a solution of crude Boc-**3j** (141 mg, 0.340 mmol) in dry CH_2Cl_2 (15 mL) was added a solution of BBr_3 in CH_2Cl_2 (1 M, 6.80 mL, 6.80 mmol) at 0 °C, and the mixture was stirred at 25 °C for 120 h. Iced water was then added and the suspension was stirred at 25 °C for 1 h. The solid was filtered and washed with H_2O, then purified by dry column vacuum chromatography on silica gel (eluent CH_2Cl_2 / MeOH) and by a further recrystallization in MeOH to afford **1j** (19 mg, 5%) as orange crystals. ^{1}H NMR (400 MHz, *d*$_6$-DMSO) δ 10.15 (s, 1H), 9.95 (s, 1H), 7.86 (s, 1H), 7.66 (d, *J* = 8.6 Hz, 1H), 7.26 (t, *J* = 7.7 Hz, 1H), 6.95 (d, *J* = 7.7 Hz, 1H), 6.70 (d, *J* = 7.7 Hz, 1H),

6.43 (d, *J* = 2.3 Hz, 1H), 6.38 (dd, *J* = 8.6 Hz, 2.3 Hz, 1H), 5.84 (q, *J* = 5.0 Hz, 1H), 3.68 (s, 2H), 2.82 (d, *J* = 5.0 Hz, 3H). ^{13}C NMR (125 MHz, d_6-DMSO) δ 194.0, 160.7, 159.6, 146.7, 138.0, 135.1, 130.7, 129.7, 128.7, 127.0, 113.7, 112.2, 109.7, 107.8, 102.5, 29.8, 29.7. HRMS (ESI) *m/z* calc. for $C_{17}H_{16}NO_3$ $(M+H)^+$: 282.11247. Found: 282.11264.

Enzymatic Assays. Tyrosinase from *Agaricus bisporus* (25 kU, Sigma-Aldrich) was dissolved in phosphate buffer (200 mM, pH 7.0) and aliquoted in 500 U tubes with a final volume of 1 mL. A volume of 10 µL of this solution was seeded on 96-well plates, and treated with increasing concentrations of test compounds (dissolved in DMSO), all wells (including negative controls) receiving the same amount of vehicle (*i.e.*, 2% final concentration of DMSO (v/v)). The plate was then incubated at 25 °C for 15 min, 50 µL of L-DOPA in phosphate buffer (1.25 mM, pH 7.0) was added to each well, and the dopachrome formation was monitored by measuring absorbance at 475 nm after 5 min using a SPECTRA MAX® ABS Plus microplate reader with SoftMax Pro 7.1 software. Each experiment was performed three times, and the obtained data were treated with respect to appropriate blank (without the enzyme) and control (without the inhibitor) experiments.

MNT-1 Cell Culture. Human melanoma cells (MNT-1) were obtained from the National Institute of Health (NIH) and were grown in Dulbecco's Modified Eagle's-F12 Medium (DMEM-F12) supplemented with 10% fetal calf serum and 1% antibiotics, in 75 cm^2 ventilated flask maintained at 37 °C in a 5% CO_2 incubator. Cells were routinely passed using trypsin-EDTA solution.

Screening Against MNT-1 Lysates. Inhibition of tyrosinase by test compounds was first evaluated using cell lysate prepared from MNT-1 cells. Briefly, confluent MNT-1 cells cultivated on 75 cm^2 flasks were washed with phosphate buffer saline (PBS) and detached using trypsin-EDTA solution. Cells suspension was aliquoted in cryotubes (approximately $4{\cdot}10^6$ cells per

tube) and tubes were then centrifuged at 1,200 rpm for 5 min. Supernatants were eliminated and cells pellets were snapfrozen in liquid nitrogen before being stored at –80 °C until tyrosinase assay. Defrosted MNT-1 cell lysates were washed with 1 mL of PBS/Triton 1X and centrifuged three times at 3,000 g for 3 min. The supernatant was then extracted and diluted in PBS/Triton 1X (10 mL). A volume of 96 µL of supernatant was seeded on 96-well plates, and treated with increasing concentrations of test compounds (dissolved in DMSO), all wells (including negative controls) receiving the same amount of vehicle (*i.e.*, 2% final concentration of DMSO (v/v)). The plate was then incubated at 37 °C for 10 min, 100 µL of L-DOPA in PBS/Triton 1X (4.0 mM) was added to each well, and the melanin formation was monitored by measuring absorbance at 600 nm after 3 h using a SPECTRA MAX® ABS Plus microplate reader with SoftMax Pro 7.1 software. Each experiment was performed three times, and the obtained data were treated with respect to appropriate blank (without the lysate) and control (without the inhibitor) experiments.

MNT-1 Whole Cells Assay and Cytotoxicity. Toxicity assay was performed as previously described with some modifications.[19] Briefly, MNT-1 cells grown on 75 cm^2 flask were detached using trypsin-EDTA solution and were then plated onto 96-wells plates at the initial density of 100,000 cells per cm^2 and incubated at 37 °C in a 5% CO_2 incubator. When confluence was reached (usually 48–72 h after plating), the cell medium was changed to fresh medium and cells were treated with increasing concentrations of test compounds (dissolved in DMSO). All wells (including negative controls) were treated the same amount of vehicle (*i.e.*, 0.1% final concentration of DMSO (v/v)). The cells were then incubated for 4 or 14 days at 37 °C in a 5% CO_2 incubator. The medium of wells was changed every 2 days by aspiration and replacement with fresh medium containing increasing concentrations of molecules. At the end of the incubation, wells were aspirated and cell viability was evaluated using resazurin assay as previously described.[28] Whole cells inhibition of melanin synthesis was measured as follow. MNT-1 cells

were plated onto 12-wells plates at 100,000 cells per cm^2. Once confluence was reached (48–72 h after plating), cells were exposed to increasing concentrations of molecules (dissolved in DMSO), negative controls receiving the same amount of vehicle (*i.e.*, 0.1% final concentration of DMSO (v/v)). The cells were then incubated for 4 or 14 days at 37 °C in a 5% CO_2 incubator with medium replacement with fresh medium containing increasing concentrations of molecules every 2 days as for the toxicity assay. At the end of the incubation, cells were washed three times with cold PBS, were then mechanically detached using plastic scraper and were finally transferred to Eppendorf tubes. After centrifugation (at 1200 rpm for 5 min), cell pellets were lysed by adding 0.3 mL of lysis solution (NaOH (2 M) plus 10% DMSO) and repeated sonication/vortexing were done until complete solubilization of melanin. Cell-associated melanin contents were measured at 600 nm using pure melanin (purchased from Sigma-Aldrich) diluted in lysis solution as standard. Protein contents were measured using the Lowry's procedure, bovine serum albumin (BSA) being used as standard to allow the normalization of the melanin contents.

Molecular Modeling. A homology model of *hs*TYR built from the crystal structure of *hs*TYRP1 was retrieved from Swiss Model Expasy.[24] The docked compound and the protein were prepared using LePro tool. Compounds **1l**, **1m** and **1n** were then docked using LeDock software with standard settings, and for each ligand a total of 20 poses were generated. Only poses with low energy conformations and plausible geometries were considered. UCSF Chimera 1.14 was used to display the small molecule ligand–protein docking results. The crystal structures of tyrosinase from *Bacillus megaterium* with bound L-tyrosine and L-DOPA were retrieved from the Protein DataBank (PDB is 4P6R and 4P6S, respectively) and were superimposed with the best docking poses using UCSF Chimera 1.14.

DECLARATION OF COMPETING INTEREST

The authors declare that they have no competing financial interests or personal relationships that could have appeared to influence the work reported in this paper.

ACKNOWLEDGEMENTS

This work was supported by the ANR ("Agence Nationale de la Recherche") through Labex ARCANE and CBH-EUR-GS (ANR-17-EURE-0003) and through ANR project EPIDERMIS (ANR-19-CE44-0002). The authors thank Labex ARCANE for the fellowship grant of L.M.L in the frame of project SHAPESHIFT, the ANR for the fellowship grant of M.B. in the frame of project EPIDERMIS, and the French MESR ("Ministère de l'Enseignement supérieur, de la Recherche et de l'Innovation") for the fellowship grant of B.R.

REFERENCES

(1) Lai, X.; Wichers, H. J.; Soler-Lopez, M.; Dijkstra, B. W. Structure and function of human tyrosinase and tyrosinase-related proteins. *Chem. Eur. J.* **2018**, *24*, 47–55.

(2) Beaumet, M.; Lazinski, L. M.; Maresca, M.; Haudecoeur, R. Catechol-mimicking transition-state analogues as non-oxidizable inhibitors of tyrosinases. *Eur. J. Med. Chem.* **2023**, *259*, 115672.

(3) Pillaiyar, T.; Namasivayam, V.; Manickam, M.; Jung, S.-H. Inhibitors of melanogenesis: an updated review. *J. Med. Chem.* **2018**, *61*, 7395–7418.

(4) Roulier, B.; Pérès, B.; Haudecoeur, R. Advances in the design of genuine human tyrosinase inhibitors for targeting melanogenesis and related pigmentations. *J. Med. Chem.* **2020**, *63*, 13428–13443.

(5) Fogal, S.; Carotti, M.; Giaretta, L.; Lanciai, F.; Nogara, L.; Bubacco, L.; Bergantino, E. Human tyrosinase produced in insect cells: a landmark for the screening of new drugs addressing its activity. *Mol. Biotechnol.* **2015**, *57*, 45–57.

(6) Mann, T.; Gerwat, W.; Batzer, J.; Eggers, K.; Scherner, C.; Wenck, H.; Stäb, F.; Hearing, V. J.; Röhm, K.-H.; Kolbe, L. Inhibition of human tyrosinase requires molecular motifs distinctively different from mushroom tyrosinase. *J. Invest. Dermatol.* **2018**, *138*, 1601–1608.

(7) Desmedt, B.; Courselle, P.; De Beer, J. O.; Rogiers, V.; Grosber, M.; Deconinck, E.; De Paepe, K. Overview of skin whitening agents with an insight into the illegal cosmetic market in Europe. *J. Eur. Acad. Dermatol. Venereol.* **2016**, *30*, 943–950.

(8) Brozyna, A. A.; VanMiddlesworth, L.; Slominski, A. T. Inhibition of melanogenesis as a radiation sensitizer for melanoma therapy. *Int. J. Cancer* **2008**, *123*, 1448–1456.

(9) Slominski, A. T.; Zbytek, B.; Slominski, R. Inhibitors of melanogenesis increase toxicity of cyclophosphamide and lymphocytes against melanoma cells. *Int. J. Cancer* **2009**, *124*, 1470–1477.

(10) Buitrago, E.; Hardré, R.; Haudecoeur, R.; Jamet, H.; Belle, C.; Boumendjel, A.; Bubacco, L.; Réglier, M. Are human tyrosinase and related proteins suitable targets for melanoma therapy? *Curr. Top. Med. Chem.* **2016**, *16*, 3033–3047.

(11) Lai, X.; Soler-Lopez, M.; Wichers, H. J.; Dijkstra, B. W. Large-scale recombinant expression and purification of human tyrosinase suitable for structural studies. *PLoS One* **2016**, *11*, e0161697.

(12) Lai, X.; Wichers, H. J.; Soler-Lopez, M.; Dijkstra, B. W. Structure of human tyrosinase related protein 1 reveals a binuclear zinc active site important for melanogenesis. *Angew. Chem. Int. Ed.* **2017**, *56*, 9812–9815.

(13) Mann, T.; Scherner, C.; Röhm, K.-H.; Kolbe, L. Structure-activity relationships of thiazolyl resorcinols, potent and selective inhibitors of human tyrosinase. *Int. J. Mol. Sci.* **2018**, *19*, 690.

(14) Arrowitz, C.; Schoelermann, A. M.; Mann, T.; Jiang, L. I.; Weber, T.; Kolbe, L. Effective tyrosinase inhibition by thiamidol results in significant improvement of mild to moderate melasma. *J. Invest. Dermatol.* **2019**, *139*, 1691–1698.

(15) Dubois, C.; Haudecoeur, R.; Orio, M.; Belle, C.; Bochot, C.; Boumendjel, A.; Hardré, R.; Jamet, H.; Réglier, M. Versatile effects of aurone structure on mushroom tyrosinase activity. *ChemBioChem* **2012**, *13*, 559–565.

(16) Haudecoeur, R.; Gouron, A.; Dubois, C.; Jamet, H.; Lightbody, M.; Hardré, R.; Milet, A.; Bergantino, E.; Bubacco, L.; Belle, C.; Réglier, M.; Boumendjel, A. Investigation of the binding-site homology of mushroom and bacterial tyrosinases by aurones as effectors. *ChemBioChem* **2014**, *15*, 1325–1333.

(17) Markova, E.; Kotik, M.; Krenkova, A.; Man, P.; Haudecoeur, R.; Boumendjel, A.; Hardré, R.; Mekmouche, Y.; Courvoisier-Dezord, E.; Réglier, M.; Martinkova, L. Recombinant tyrosinase from *Polyporus arcularius*: overproduction in *Escherichia coli*, characterization, and use in a study of aurones as tyrosinase effectors. *J. Agric. Food Chem.* **2016**, *64*, 2925–2931.

(18) Haudecoeur, R.; Carotti, M.; Gouron, A.; Maresca, M.; Buitrago, E.; Hardré, R.; Bergantino, E.; Jamet, H.; Belle, C.; Réglier, M.; Bubacco, L.; Boumendjel, A. 2-Hydroxypyridine-*N*-oxide-embedded aurones as potent human tyrosinase inhibitors. *ACS Med. Chem. Lett.* **2017**, *8*, 55–60.

(19) Roulier, B.; Rush, I.; Lazinski, L. M.; Pérès, B.; Olleik, H.; Royal, G.; Fishman, A.; Maresca, M.; Haudecoeur, R. Resorcinol-based hemiindigoid derivatives as human tyrosinase inhibitors and melanogenesis suppressors in human melanoma cells. *Eur. J. Med. Chem.* **2023**, *246*, 114972.

(20) Lazinski, L. M.; Royal, G.; Robin, M.; Maresca, M.; Haudecoeur, R. Bioactive aurones, indanones, and other hemiindigoid scaffolds: medicinal chemistry and photopharmacology perspectives. *J. Med. Chem.* **2022**, *65*, 12594–12625.

(21) Howlader, A. H.; Diaz, K.; Mebel, A. M.; Kaiser, R. I.; Wnuk, S. F. Iodoindenes: synthesis and application to cross-coupling. *Tetrahedron Lett.* **2020**, *61*, 152427.

(22) Haudecoeur, R.; Ahmed-Belkacem, A.; Yi, W.; Fortuné, A.; Brillet, R.; Belle, C.; Nicolle, E.; Pallier, C.; Pawlotsky, J.-M.; Boumendjel, A. Discovery of naturally occurring aurones that are potent allosteric inhibitors of hepatitis C virus RNA-dependant RNA polymerase. *J. Med. Chem.* **2011**, *54*, 5395–5402.

(23) Lai, X.; Wichers, H. J.; Soler-Lopez, M.; Dijkstra, B. W. Structure of human tyrosinase related protein 1 reveals a binuclear zinc active site important for melanogenesis. *Angew. Chem. Int. Ed.* **2017**, *56*, 9812–9815.

(24) P14679 Homo sapiens tyrosinase model. https://swissmodel.expasy.org/repository/uniprot/P14679 (Accessed 11 July 2023).

(25) Çinaroglu, S. S.; Timuçin, E. Comparative assessment of seven docking programs on a nonredundant metalloprotein subset of the PDBbind refined. *J. Chem. Inf. Model.* **2019**, *59*, 3846–3859.

(26) Kampatsikas, I.; Pretzler, M.; Rompel, A. Identification of amino acid residues responsible for C–H activation in type-III copper enzymes by generating tyrosinase activity in a catechol oxidase. *Angew. Chem. Int. Ed.* **2020**, *59*, 20940–20945.

(27) Goldfeder, M.; Kanteev, M.; Isaschar-Ovdat, S.; Adir, N.; Fishman, A. Determination of tyrosinase substrate-binding modes reveals mechanistic differences between type-3 copper proteins. *Nat. Commun.* **2014**, *5*, 4505.

(28) Olleik, H.; Nicoletti, C.; Lafond, M.; Courvoisier-Dezord, E.; Xue, P.; Hijazi, A.; Baydoun, E.; Perrier, J.; Maresca, M. Comparative structure–activity analysis of the antimicrobial activity, cytotoxicity, and mechanism of action of the fungal cyclohexadepsipeptides enniatins and beauvericin. *Toxins* **2019**, *11*, 514.